The footprints of ancient CO_2-driven flow systems: Ferrous carbonate concretions below bleached sandstone

David B. Loope* and Richard M. Kettler
Department of Earth and Atmospheric Sciences, University of Nebraska, Lincoln, Nebraska 68588, USA

ABSTRACT

Iron-rich carbonates and the oxidized remains of former carbonates (iron-oxide concretions) underlie bleached Navajo Sandstone over large portions of southern Utah. Iron in the carbonates came from hematite rims on sand grains in the upper Navajo that were dissolved when small quantities of methane accumulated beneath the sealing Carmel Formation. As a second buoyant gas (CO_2 derived from Oligocene–Miocene magmas) reached the seal and migrated up dip, it dissolved in the underlying water, enhancing the solution's density. This water carried the released ferrous iron and the methane downward. Carbonates precipitated when the descending, reducing water degassed along fractures. The distribution of a broad array of iron-rich features made recognition of the extent of the ancient flow systems possible. Although siderite is not preserved, dense, rhombic, mm-scale, iron-oxide pseudomorphs after ferrous carbonates are common. Distinctive patterns of iron oxide were also produced when large (cm-scale), poikilotopic carbonate crystals with multiple iron-rich zones dissolved in oxidizing waters. Rhombic pseudomorphs are found in the central cores of small spheroids and large (meter-scale), irregular concretions that are defined by thick, tightly cemented rinds of iron-oxide–cemented sandstone. The internal structure and distribution of these features reveal their origins as iron-carbonate concretions that formed within a large-scale flow system that was altered dramatically during Neogene uplift of the Colorado Plateau. With rise of the Plateau, the iron-carbonate concretions passed upward from reducing formation water to shallow, oxidizing groundwater flowing parallel to modern drainages. Finally they passed into the vadose zone. Absolute dating of different portions of these widespread concretions could thus reveal uplift rates for a large portion of the Plateau. Iron-rich masses in other sedimentary rocks may reveal flow systems with similar histories.

INTRODUCTION

Over a broad portion of the Colorado Plateau of southwestern United States, the Jurassic Navajo Sandstone contains a wide variety of iron-oxide–cemented masses. Here we explain why these structures are found down section and down dip from bleached sandstone. When carbon dioxide dissolves in an aqueous solution, the density of that solution increases. This fact has huge implications for subsurface carbon sequestration (Lindeberg and Wessel-Burg, 1997; Ennis-King and Paterson, 2005; MacMinn and Juanes, 2013), and here we show that it is essential to understanding iron diagenesis in the Navajo Sandstone.

North of the Grand Canyon, in southern Utah's Grand Staircase, the upper part of the Navajo Sandstone forms the White Cliffs and the lower Navajo forms the upper part of the Vermillion Cliffs (Fig. 1). Mudrocks and evaporites of the Middle Jurassic Carmel Formation form an effective seal at the top of the Navajo. Previous workers have shown that the upper Navajo was originally red and that the iron in the concretions came from iron liberated during the bleaching of the overlying rocks (Beitler et al., 2005; Chan et al., 2005). We agree with these conclusions, but they raise two previously unanswered questions: How, if the iron-oxide concretions came from the bleached rocks above, was the iron moved down section and down dip? And, if the concretions formed as primary precipitates from the mixing of reducing and oxidizing waters (Beitler et al., 2005; Chan et al., 2005), how was oxidizing water introduced and maintained below the widespread reducing waters?

In this paper, we present a conceptual model for bleaching of the sandstone and the downward transport of iron from the source rock to the geochemical trap where concretions nucleated and grew. First, we will describe and interpret a variety of iron-rich concretions. Some still contain carbonate minerals and some do not, but we argue below that all originated as reduced-iron carbonates. The bleached rocks are striking evidence for a large-scale flow system (Beitler et al., 2005; Chan et al., 2005). We claim that the concretions reveal the changing composition, source, oxidation state, and migration direction of the fluids in that system.

In the Ladbroke Grove Gas Field (Otway Basin, South Australia), the Cretaceous sandstone reservoir contains high levels of CO_2 that was derived from a magmatic source (Watson et al., 2004). In a nearby gas field, the same sandstone is not exposed to CO_2-enhanced pore waters. Analysis of cores shows that iron-rich carbonate minerals are much more abundant in the former reservoir than in the latter. These pore-filling carbonates occur mostly as concretions 2–10 cm in diameter. The Ladbroke Grove Field is an excellent analog for geological storage of CO_2 (Watson et al., 2004), and we argue here that—before it was exhumed during the Neogene—the Navajo Sandstone contained CO_2, methane, and abundant, iron-rich carbonate concretions.

Ferrous iron, carbon dioxide, methane, and siderite have been widespread in the pore waters of Earth's sediments and sedimentary rocks for billions of years, but iron oxides have been widespread on Earth only since the Early Proterozoic. Recognition that iron-oxide masses in the Navajo Sandstone had ferrous carbonate precursors (Loope et al., 2010, 2011, 2012; Kettler et al., 2011; Weber et al., 2012) and that those carbonates were emplaced by CO_2-driven flow systems should aid interpretation of other iron-oxide accumulations on Earth and on other planets.

*Corresponding author email: dloope1@unl.edu

Geosphere; June 2015; v. 11; no. 3; doi:10.1130/GES01094.1; 12 figures; 1 table.
Received 26 June 2014 ♦ Revision received 20 January 2015 ♦ Accepted 25 March 2015

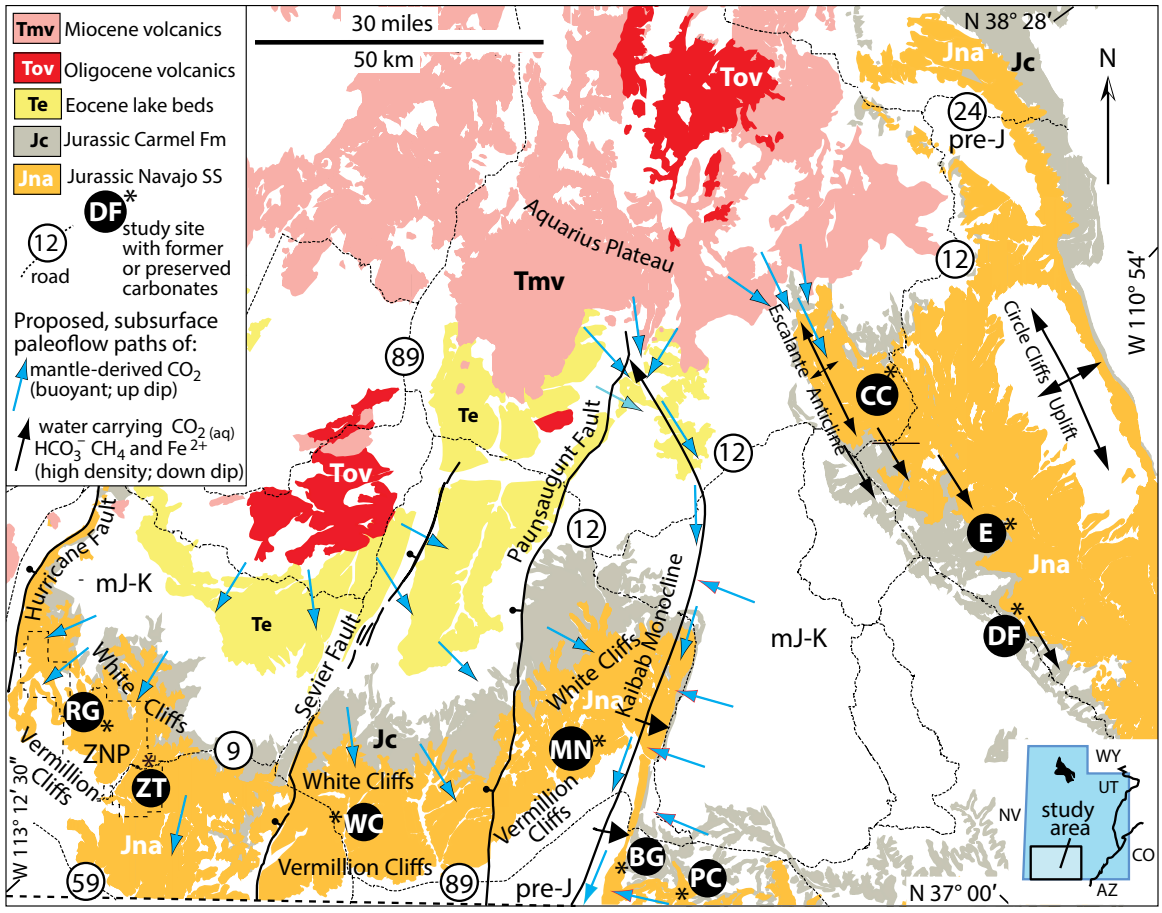

Figure 1. Simplified geologic map of southwestern Utah showing distribution of Mesozoic and Cenozoic rocks, major structures, locations of study sites, and postulated, subsurface paleoflow paths of buoyant, supercritical CO_2 and, in the eastern part of study area, paths of dense water carrying ferrous iron and aqueous CO_2 (alternative explanation for the eastern paths [black arrows] is hydrodynamic flow; Loope et al., 2010). Flow paths of dense waters in the western area are unknown. SH—Sand Hollow; RG—Russell Gulch; ZT—Zion Tunnel; 3LC—Three Lakes Canyon; MN—Mollie's Nipple; BG—Buckskin Gulch; PC—Paria Canyon; CC—Calf Creek; E—Egypt; DF—Dry Fork. ZNP near southwest corner is Zion National Park. For generalized cross section of the Grand Staircase: http://en.wikipedia.org/wiki/Grand_Staircase-Escalante_National_Monument#mediaviewer/File:Grand_Staircase-big.jpg.

Previous Work

Chan et al. (2000, 2005), Beitler et al. (2005), and Nielsen et al. (2009) carried out extensive studies on both the bleaching of the Navajo Sandstone and the iron-oxide concretions within it. Nielsen et al. (2009) showed that although the upper Navajo Sandstone is bleached in the southern part of Zion National Park (and continuously for 100 km eastward; Fig. 1), bleaching does not extend to the northwestern portion of Zion, where the Navajo retains its early diagenetic, red color. Although this color-transition zone is only ~2 km wide, it does not appear to be structurally controlled (Nielsen et al., 2009, p. 84). Beitler et al. (2005) proposed that the iron-oxide concretions are primary precipitates formed during the mixing of iron-bearing, reducing waters and oxygenated meteoric waters. This hypothesis guided field-based work (Potter and Chan, 2011), bench experiments (Chan et al., 2007; Barge et al., 2011), and iron isotope studies (Chan et al., 2006; Busigny and Dauphas, 2007). Loope et al. (2010, 2011, 2012) and Kettler et al. (2011) reinterpreted the concretions as the altered (oxidized) remains of precursor concretions cemented by ferrous carbonate minerals. Weber et al. (2012) presented evidence that iron-oxidizing microbes mediated the oxidation of the carbonates. Reiners et al. (2014) measured (U-Th)/He ages and element concentrations in iron oxide from Navajo cements, concretions, and fracture fills.

Study Area and Geologic Setting

This paper is based on field observations and analyses of four different types of samples from the Navajo Sandstone at ten localities (Fig. 1): (1) rinded, iron-oxide–cemented concretions; (2) sandstone with poikilotopic, iron-zoned ferroan calcite cement; (3) calcite concretions containing large, rhombic, iron-oxide pseudomorphs or iron-oxide accumulations along cleavage planes; and (4) iron-oxide patterns preserved in non-calcareous sandstone. Three of our sites (Fig. 1) are down dip from the Escalante and Circle Cliffs Anticlines, along the flow path defined by pipe-like concretions in the Navajo Sandstone (Loope et al., 2010). Two lie along the east flank of the Kaibab

upwarp, and four other sites are in flat-lying strata below the White Cliffs west of the Kaibab monocline and east of the Hurricane fault. One site occupies part of a gentle syncline, just west of the Hurricane fault (SH, Fig. 1).

The Navajo Sandstone was deposited near the western edge of Pangea in a vast, Early Jurassic sand sea (Kocurek and Dott, 1983). Large-scale cross strata composed of wind-ripple and dry avalanche (grain-flow) deposits make up more than 95% of the formation. In contrast to many marine and fluvial depositional environments, organic matter was very sparse in the Navajo erg, so pore waters remained oxidizing long after deposition.

The study area lies within the west-central Colorado Plateau, in the transition zone to the Basin and Range Province to the west. The Kaibab upwarp, Circle Cliffs upwarp, and the Escalante anticline are compressional, Laramide structures that developed 80–40 Ma, above reverse faults in basement rocks. Dickinson et al. (2012) showed that the eroded nose of the Kaibab upwarp was buried by flat-lying, Middle Eocene (ca. 40 Ma) lacustrine strata that now crop out at high elevation in the northern part of the study area (Fig. 1). The Navajo Sandstone has been eroded from the southern portion of the Kaibab upwarp, and Permian Kaibab Limestone is exposed along its crest.

At least 11 Colorado Plateau anticlines presently contain large volumes of carbon dioxide (Haszeldine et al., 2005). Gilfillan et al. (2008) studied the noble gas geochemistry of five natural CO_2 reservoirs from the Colorado Plateau and Rocky Mountain provinces and concluded that the dominant sources of all fields were magmatic. In the transition zone to the Basin and Range Province, explosive igneous activity was widespread on the Plateau during middle and late Cenozoic time. The lavas exposed in the northern part of our study area (Fig. 1) are part of the Marysvale volcanic field, one of the largest in western United States. Most calc-alkaline magmatic activity occurred during the Oligocene and Miocene (32–22 Ma), and the less voluminous bimodal basalts and rhyolites were emplaced as recently as the Holocene (Rowley et al., 2002). The Marysvale field is at the eastern edge of a caldera complex that was centered on what is now the Basin and Range Province. Some of the springs located along faults in the Grand Canyon issue mantle-derived CO_2 and helium (Crossey et al., 2006, 2009). Work on springs and travertines shows that although some portions of these gases reflect ongoing processes in the asthenosphere, another strong component was released during the Oligocene (Crossey et al., 2009).

Near the town of Green River, Utah, carbon dioxide has been escaping for hundreds of thousands of years from a faulted reservoir in the Navajo Sandstone (Shipton et al., 2005; Heath et al., 2009; Burnside et al., 2013). Wigley et al. (2012) and Kampman et al. (2014) showed that the escaping fluid has extensively bleached the overlying Jurassic Entrada Sandstone and that ferroan carbonates are forming at the reaction front between bleached and unbleached sandstone.

Three major, N-S–trending normal faults cut Mesozoic rocks of the study area (Fig. 1). Initial movement along the Hurricane and Sevier faults was probably 15–12 million years ago (Late Miocene; Davis, 1999); the youngest rocks cut by Paunsaugunt fault are 20 million years old (Bowers, 1991). Offset along these faults clearly postdates bleaching of the Navajo Sandstone (Nielsen et al., 2009).

Our three westernmost study sites lie within the western Grand Canyon volcanic field, an area with hundreds of basaltic cinder cones and lava flows (Karlstrom et al., 2007; Crow et al., 2008; Karlstrom et al., 2012). The flows closest to our sites range in age from 1.4 million years to less than 100,000 years (Biek et al., 2003). Most of these flows were emplaced during a single eruptive cycle (Smith et al., 1999), and many flowed down paleovalleys and now cap ridges because of their high resistance to erosion (the inverted valleys of Hamblin, 1970).

In the past six million years, the Colorado Plateau has been uplifted ~2 km (Pederson et al., 2002; Karlstrom et al., 2012, 2014). During uplift, pore waters of the Navajo Sandstone—previously buried by thousands of meters of younger strata—were recharged by rain and snow that fell on the high plateaus of the northern part of the study area. This study reports observations of rocks exposed on canyon walls, but a large percentage of the Navajo remains below the regional water table. Parry et al. (2009) reported ferrous carbonate minerals in Navajo Sandstone cores from the Covenant oil field in central Utah.

LATE DIAGENETIC CONCRETIONS AND CEMENTS

Rinded Iron-Oxide–Cemented Concretions

Ironstones, spheroids, boxworks, and pipes defined by isopachous rinds or shells that are densely cemented by iron oxide (Figs. 2 and 3) are widespread in the Navajo Sandstone. At Russell Gulch, in west-central Zion National Park, rinded concretions are present in two of the diagenetic subfacies defined by Nielsen et al. (2009)—the pink altered subfacies that is prevalent in the middle Navajo and the brown ferruginous subfacies in the lower Navajo. Rinds vary from less than 1 mm to 3 cm in thickness, and the sandstone surrounded by rinds can be iron poor. In many concretions, however, centrally located cores contain abundant iron-oxide cement. Some of this cement forms dense, rhombic pseudomorphs (Fig. 2; Loope et al., 2011; Kettler et al., 2011). The outer (rind) portion of massive ironstones at Russell Gulch is composed of mm-scale, crinkled bands of iron-oxide–cemented sandstone, and cross sections of some of these large masses reveal non-banded cores (Fig. 3A). Parallel, iron-oxide streaks or "comet tails" extend from many spheroids, and the azimuths of the streaks are parallel to the trends of elongate, pipe-like concretions in nearby outcrops (Fig. 4). At Calf Creek, boxworks are surrounded by thick iron-oxide rinds and contain additional rinds where small joints are present within the structure (Fig. 3B).

Pipe-like concretions composed of thousands of iron-rich, cm-scale, non-calcareous spheroids are abundant at Sand Hollow (Figs. 3C and 3D). Centimeter-thick, iron-oxide–cemented rinds delineate the perimeters of many of these pipes. Pipes are developed in the plane of cross bedding; their trends are oblique to both the strike and dip direction of cross beds.

Interpretation of Rinded Concretions

The rinded, iron-oxide–rich concretions in the Navajo Sandstone are the oxidized remains of concretions that were originally cemented by siderite ($FeCO_3$). Our previous work (Loope et al., 2010, 2011, 2012; Kettler et al., 2011) has emphasized the importance of siderite in the origin of concretions defined by dense, iron-oxide rinds or shells that surround uncemented centers. Weber et al. (2012) presented evidence that the rinds on the Navajo concretions are biosignatures of iron-oxidizing microbes that mediated the dissolution and oxidation of siderite.

The presence of iron-oxide rinds along closely spaced, vertical joints cutting the large concretions at Calf Creek (Fig. 3B; Loope et al., 2011) may help to constrain timing of siderite oxidation in these rocks to the late Neogene. Fossen (2007, 2010) hypothesized that, while they were buried at depths greater than ~1 km, relatively few joints cut the porous and permeable reservoir sandstones of the Colorado Plateau; the closely spaced joints in the sandstones formed only after these rocks underwent uplift and cooling (Fossen, 2010). Because the Plateau was uplifted 2 km in the past six million years (Karlstrom et al., 2014), many of the joints in these sandstones may have formed in the late Neogene.

Using laboratory experiments, Chan et al. (2007) attempted to show that spheroidal, iron-oxide rinds in the Navajo Sandstone could have formed as primary precipitates. They showed

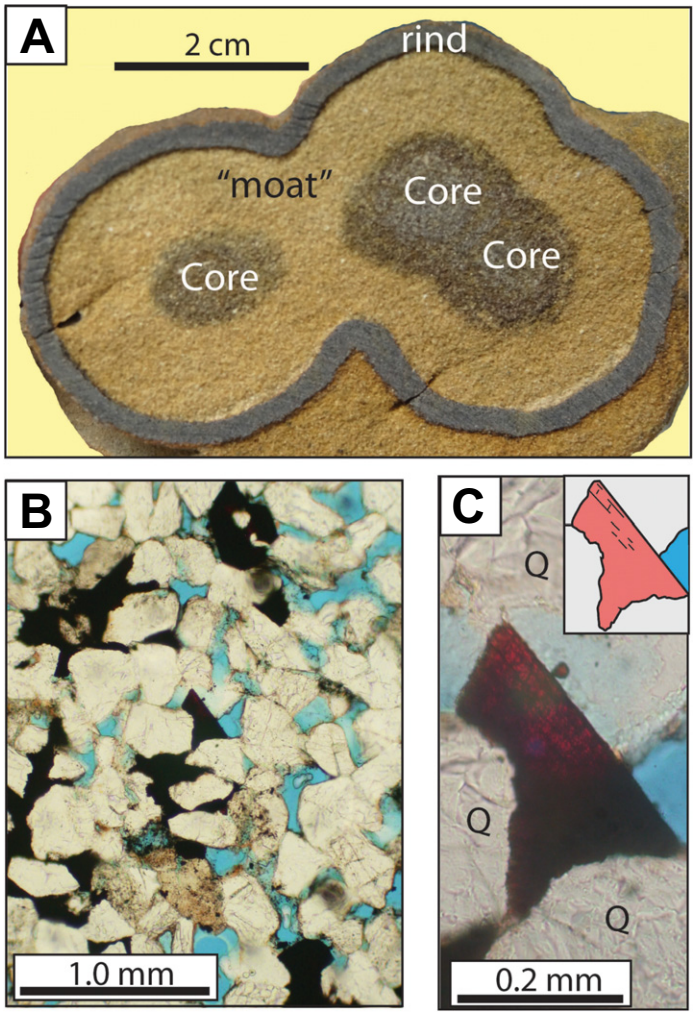

Figure 2. Spheroidal concretions with iron-oxide rinds (site RG, Fig. 1). (A) Sawed concretion with well-developed rind, iron-poor sandstone "moat," and three central cores. In the first stage (reducing pore water), three siderite concretions nucleated at nearby sites and, with continued growth, merged to form a single mass. In the second stage (oxidizing water), iron oxide precipitated on the perimeter of the mass and progressively thickened inward as the siderite was dissolved and receded. Rind thickening ended when mass entered the vadose zone. (B) Small, dense, rhomb-shaped iron-oxide accumulations cementing sand grains within the core zone of concretion; these are interpreted as pseudomorphs after siderite (surviving evidence of the first stage of concretion formation). (C) Closer view of B (with condenser) shows preserved cleavage planes within pseudomorph. Sand grains are quartz, and blue is pore-filling epoxy.

that if, in an agar matrix, an $Fe(NO_3)_3$ solution is placed adjacent to and surrounded by a KOH solution, iron hydroxide will precipitate at the reaction front. Iron diffuses outward, a circular rind forms, and the rind thickens inward as long as iron continues to diffuse from the center. We argue that this experiment demonstrates the importance of a preexisting (primary) concentration of iron in the center of the structure prior to (secondary) rind formation. The ferric iron neutralizes the base (KOH) that served as a chemical trap. In our model (Loope et al., 2010; Weber et al., 2012), a dissolving siderite concretion provides diffusing ferrous iron ions that are trapped at a surrounding, redox gradient.

Complex rinds such as the convoluted one shown in Figure 2A illustrate another reason why rinds cannot be primary precipitates—two steps, two iron minerals, and two diagenetic environments are required (Fig. 5). Under reducing conditions, closely spaced, siderite-cemented concretions nucleated and grew to form an amalgamated mass. In the laboratory, Barge et al. (2011) generated intergrown masses of analogous, self-organized spheroids cemented by silver chromate. We view their experiment as a reasonable demonstration of the first step in rind formation (precipitation of primary, intergrown spheroids—in the Navajo case, these were composed of the reduced iron mineral, siderite). The second step began as the Navajo pore water became oxygenated. Iron-oxidizing microbes colonized the convoluted, outer surface of the already-fused siderite spheroids (Fig. 5). The microbes slowly dissolved the siderite, and ferrous iron diffused to the perimeter, where it combined with oxygen. Iron oxide precipitated, forming a single, inward-thickening rind. Such a rind is thus a product of "batch processing"—its overall geometry reflects the shape of a preexisting template composed of multiple, intergrown spheroids. If the rinds had originated de novo (without a template), they would now show a growth sequence (Fig. 5D) in which new spheroidal rinds were built upon the surfaces of older rinds (a pattern in which spheroids shared walls, as is seen in soap bubbles). Intergrown Navajo spheroids do not, however, share walls (Fig. 2). Iron-rich cores within these spheroids (Fig. 2; previously unreported from the Navajo) provide new evidence supporting our model; the cores are the corroded remains of the larger, original template (Fig. 5).

The southwest-directed "comet-tails" on the Russell Gulch spheroids and nearby pipe-like concretions (Fig. 4) show that alteration of the siderite took place within groundwater that was flowing southwestward. This is the same paleoflow direction as that shown by a Late Pleistocene lava flow that filled a nearby paleovalley (Fig. 2A).

Previous studies have shown that rinds can form on other kinds of geologic templates. Following van der Burg (1969), Loope et al. (2012) showed that spindle-shaped intraclasts that form lag gravels in fluvial channels of the Cretaceous Dakota Formation (eastern Nebraska) were originally composed of sideritic floodplain silt and developed rinds only after they were deposited in the channels. The abraded shapes of the transported Dakota intraclasts dictated the shapes of the rinds that formed after transport and now surround them.

Within the cores of spheroids, ironstones, and boxworks, the oxidized remains of the original iron-carbonate crystals are preserved as rhombic

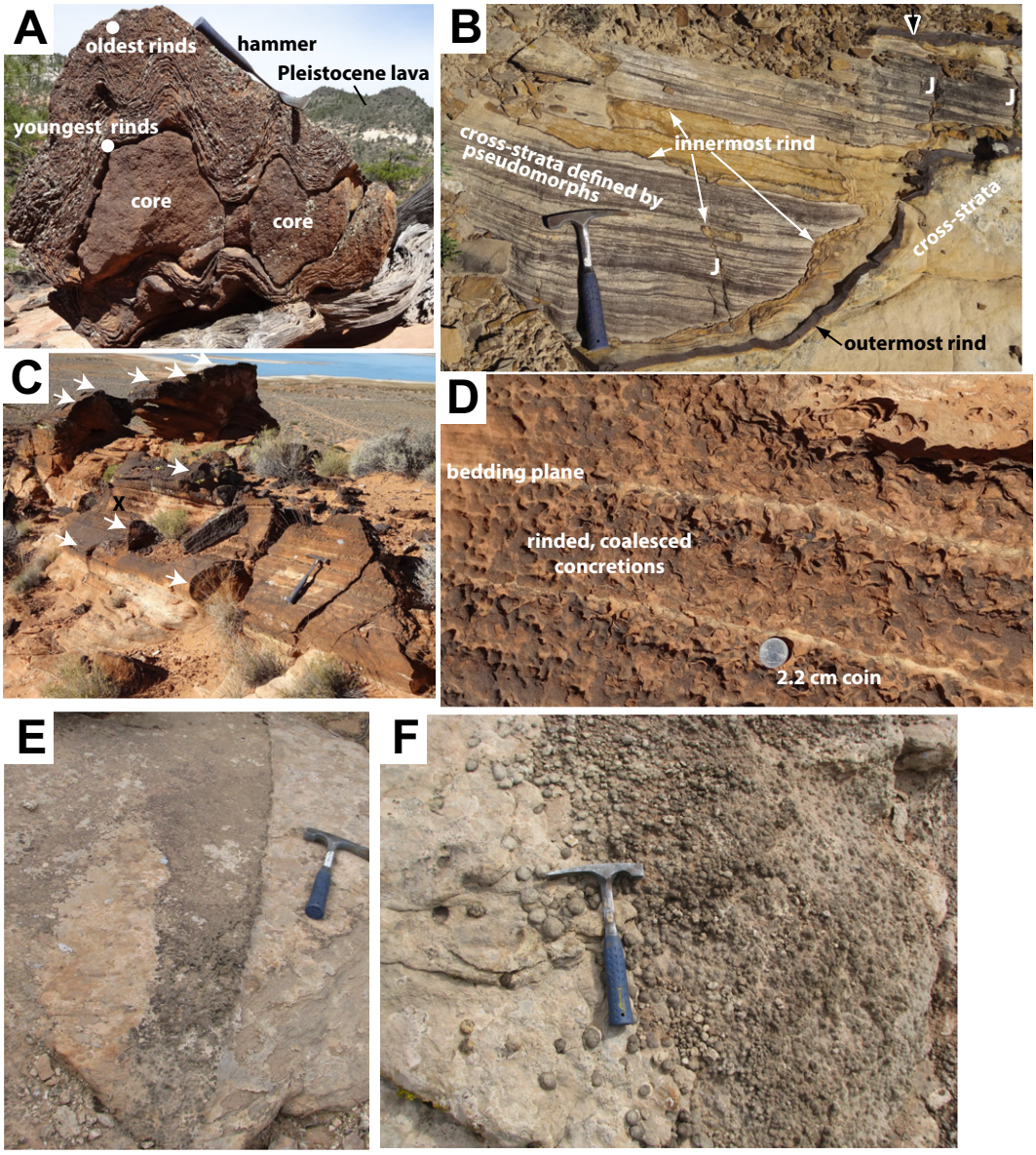

Figure 3. Large, rinded, iron-rich masses. Hammer is 28 cm long. (A) Block that fell from an adjacent, giant, in situ ironstone mass in the middle Navajo Sandstone with a very thick, laminated rind bounded on its inner surface by an irregular dissolution surface that surrounds a non-rinded core. As with smaller concretions, iron was initially concentrated by growth of a ferrous carbonate concretion; the carbonate was later oxidized from the perimeter inward. Concretion lies below the contact between valley-filling Pleistocene lava and Navajo Sandstone (Site RG, Fig. 1). (B) In situ iron-rich mass with thick outer (oldest) rind that surrounds multiple younger, thinner rinds and a complexly corroded core. Note that some thin rinds follow small joints (J). These joints are interpreted as being very young (late Neogene), postdating formation of a large iron-carbonate concretion (first stage, Fig. 2). Oxidizing waters, following bedding and joints, dissolved the carbonates and supported iron-oxidizing microbes that formed the rinds (second stage, Fig. 2). Preservation of rhombic pseudomorphs in the core suggests it was oxidized above the local water table (see Discussion) (site CC, Fig. 1). (C) Large, pipe-like concretions (white arrows) composed of cm-scale, coalesced, non-calcareous concretions. Perimeters of large pipes are delineated by dense, 1-cm-thick, iron-oxide–cemented rinds (site SH, Fig. 1). Pipes nucleated and grew parallel to the plane of cross-stratification, oblique to direction of both dip and strike. X marks site of photo D. (D) Close-up of cm-scale, non-calcareous, spheroidal concretions cemented by iron oxides that comprise the interiors of the pipe-like concretions in C. (E) Large, pipe-like concretionary mass (Entrada Sandstone, SE Utah; cf. Garden et al., 2001, fig. 5) composed of spheroidal, cm-scale concretions cemented by ferroan calcite. (F) Close-up of E showing irregular margin of pipe. Interpretation: Unlike the Navajo concretions in C and D, this Entrada pipe does not have a thick, iron-oxide rind because ferroan calcite (unlike siderite) does not undergo complete dissolution in oxygenated water and does not support the growth of iron-oxidizing microbes.

pseudomorphs after siderite or ankerite (Figs. 2 and 3). Pseudomorphs are restricted to the cores of these concretions and are never visible in the rinds. Rinds formed and thickened only when ferrous iron could diffuse away from the dissolving (sideritic) centers. We interpret the pseudomorph-bearing cores as in situ products of abiotic oxidation of siderite that took place in the vadose zone after cm-scale diffusion of ferrous iron ceased (see Discussion and Fig. 12).

The large, pipe-like concretions at Sand Hollow (Fig. 3C) that are internally composed of thousands of cm-scale spheroids (Fig. 3D) resemble the ferroan-calcite–cemented concretionary pipes that Garden et al. (2001) described from the Entrada Sandstone and interpreted as products of CO_2 degassing (Figs. 3E and 3F). The Navajo spheroids, however, are different in that they are non-calcareous and are surrounded by thick iron-oxide rinds. We argue that these differences can be attributed to the fact that siderite (unlike ferroan calcite) dissolves completely in oxygenated water of near-neutral pH.

Poikilotopic, Iron-Zoned Ferroan Calcite Crystals

At Egypt and Dry Fork, large (up to 10 m in diameter), dark concretionary masses of calcite-cemented, cross-bedded sandstone

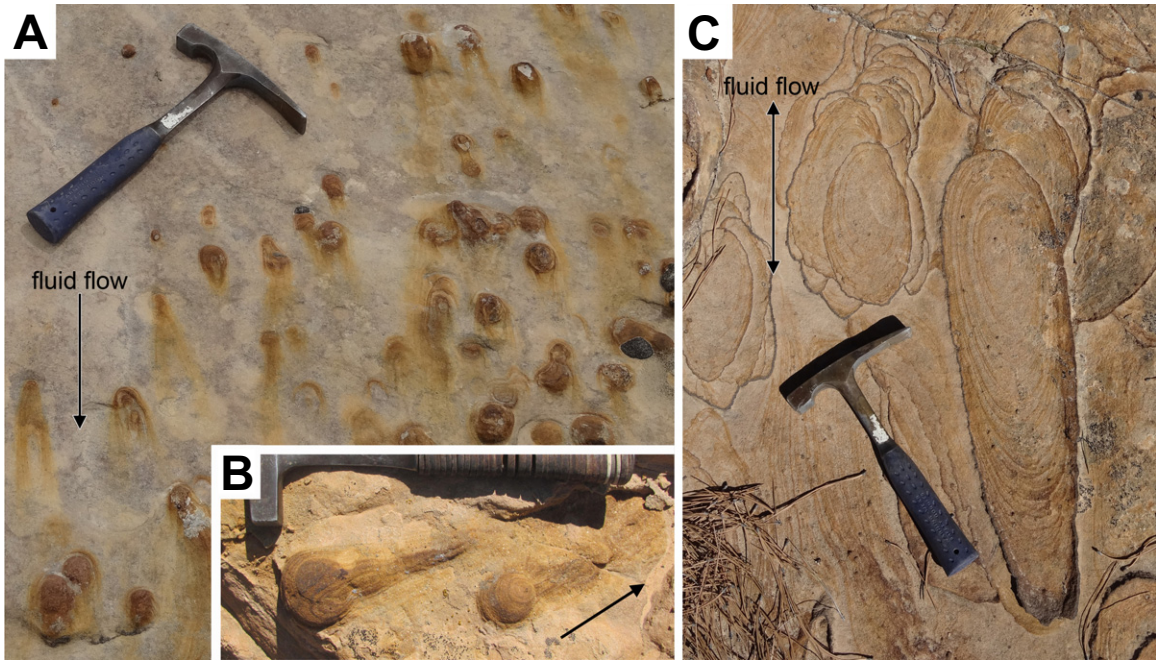

Figure 4. Flow-direction indicators for oxidizing groundwater (site RG, Fig. 1). (A) Streaks ("comet tails") extending southwestward, away from spheroidal concretions. (B) Outcrop showing that comet tails are three-dimensional structures preserved in the rock, not surficial stains. (C) Pipe-like concretions (defined by thin rinds of iron-oxide cement) that trend NE–SW. Note that these elongate rinds share walls and formed sequentially as the conduits carrying oxygenated water expanded radially into a reduced, siderite-bearing aquifer (see Loope et al., 2011, fig. 8). See Figure 12 for relationship of flow direction of oxidizing water to flow direction of Pleistocene basalt.

are nucleated on numerous shear fractures and accompanying horsetail fractures (Fig. 6A; Fossen, 2010). These structures weather into strong relief, are associated with bleached sandstone, and trend N70°W—parallel to two normal faults in the Navajo Sandstone directly east of Egypt (Utah Geological Survey, 2014). Centimeter-scale, poikilotopic calcite "sand crystals" cement the bands and surrounding bedrock (Fig. 6B). Modern lags composed of individual or twinned crystals are widespread. Individual crystals are hexagonal in cross section. Surface weathering of the individual crystals reveals concentric iron-rich zones (Fig. 6B). The $\delta^{13}C$ values of poikilotopic ferroan calcite from Egypt range from –2.78‰ to –3.48‰ (Table 1).

Interpretation of Poikilotopic, Iron-Zoned Ferroan Calcite Cement

Ferroan calcite can be preserved in a system where siderite and ankerite are dissolved because, in a mineral where only a small percentage of the divalent cations are ferrous iron, the amount of acid produced upon oxidation is small compared to the total buffering capacity of the mineral (Loope et al., 2010). The presence of iron in the calcite crystal lattice indicates this cement was precipitated from reducing pore water. As with

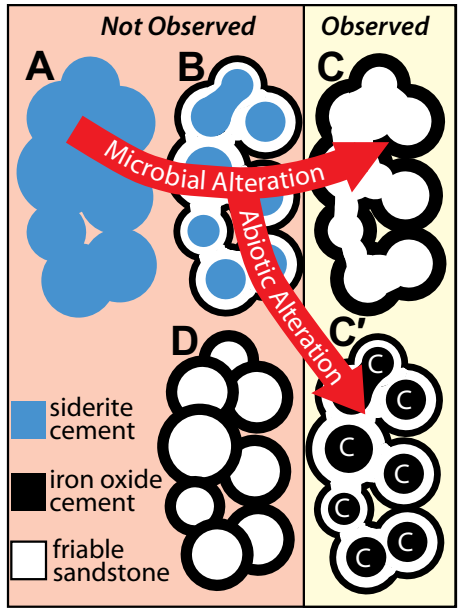

Figure 5. Evolution of rinded and cored concretions. Siderite concretions (A) nucleated in reducing water at closely spaced sites and became intergrown. When oxidizing water started to invade, iron-oxidizing microbes colonized the perimeter of the concretion (Weber et al., 2012). As metabolism proceeded, an iron-oxide rind formed on the outer surface of the concretion and thickened inward as dissolution caused the siderite to recede (B). No siderite is observed today on outcrop; the siderite of some concretions was completely exploited by the microbes (C); other concretions (C′) have oxidized cores (c) with abundant iron-oxide pseudomorphs after siderite. Note thinner rind of C′ compared to C. Interpretation: cored concretions emerged into the vadose zone before the dissolution of siderite and the diffusion of ferrous iron to the rind were complete. A concretion composed of iron-oxide rinds could theoretically form via a single process over thousands of years, within a single diagenetic environment (mixing of oxidizing and reducing water; Chan et al., 2007). We argue that such a concretion (D) would have shared (rind) walls, showing that the larger mass formed in a decipherable time sequence (similar to soap bubbles). In this example, older rinds are present at the bottom, and younger at the top. Spheroidal concretions in the Navajo Sandstone do not share walls; the observed rinds formed via a batch process—the intergrown precursor (cemented by siderite) formed over a long period of time in a single diagenetic environment and only later (in a second diagenetic environment) acted as a template for the (secondary) iron-oxide–cemented rind.

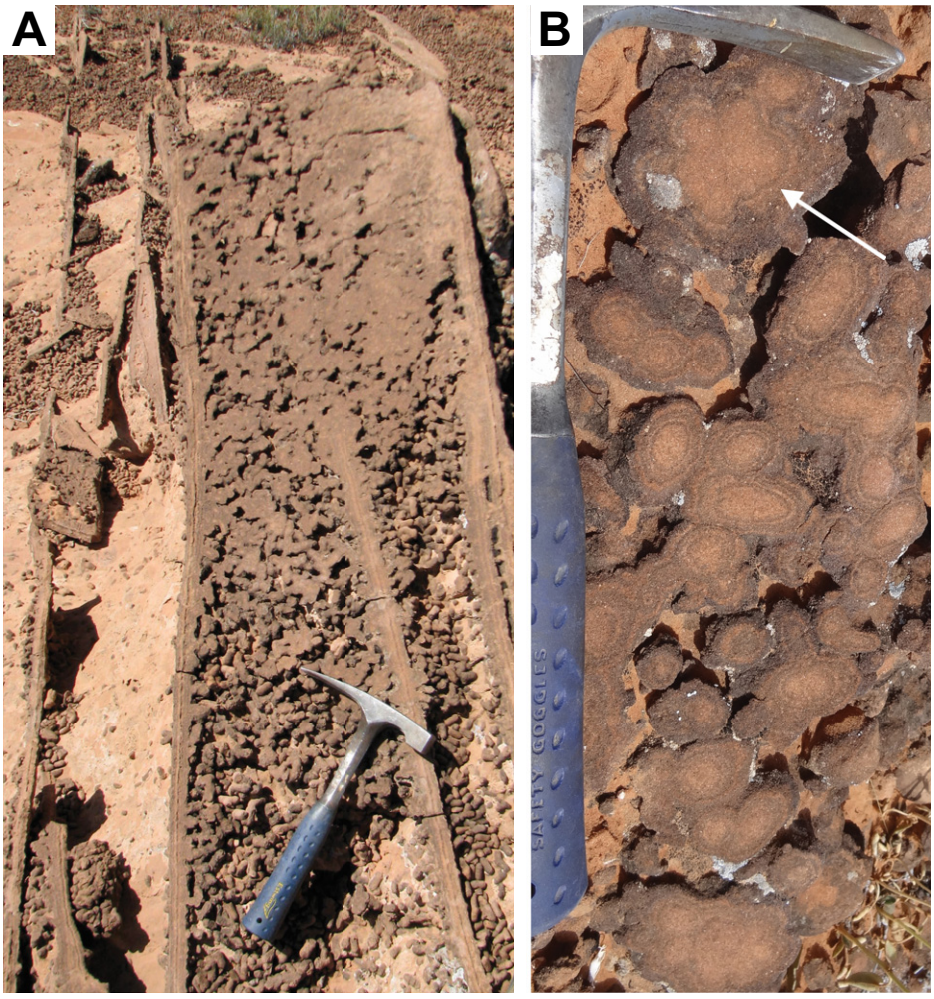

Figure 6. Concretions cemented by poikilotopic ferroan calcite (site E, Fig. 1). (A) Coarse calcite cementing horsetail fractures. (B) Large poikilotopic calcite "sand crystals" that engulfed hundreds of sand grains. Dark bands are iron-rich zones. Note that some iron-rich zones encircle numerous intergrown sand crystals (white arrow).

boxworks and pipe-like concretions in the Navajo that are associated with joints (Loope et al., 2010), the association of this ferroan calcite with brittle fractures indicates that the ferroan calcite cements are late diagenetic. In a nearby field area, Parry et al. (2004) concluded that reducing water bleached portions of the Navajo Sandstone that surround deformation bands during the early, dilational stages of the bands when their permeability was enhanced. Precipitation of the copious ferroan calcite adjacent to the fractures in our field area may have been localized by a rise in alkalinity of the pore water due to degassing of CO_2. Although methane was likely the reductant that bleached the sandstone, the relatively high $\delta^{13}C$ values present in these calcite cements indicate that methane was not the major source of carbon in their formation (Wigley et al., 2012).

TABLE 1. LOCATIONS, DESCRIPTIONS, AND ISTOPIC DATA FOR CALCITE SAMPLES

Location	Sample no.	Description	$\delta^{13}C$ (‰ VPDB)	$\delta^{18}O$ (‰ SMOW)
Egypt	1	Calcite sand crystal	–2.78	12.90
Egypt	2	Calcite sand crystal	–2.81	13.70
Egypt	3	Calcite sand crystal	–3.48	13.26
Dry Fork	1	White discoid	–1.58	11.01
Dry Fork	2	White discoid	–3.07	11.76
Paria Canyon	1	Large spheroid	–4.97	17.13

Note: See Figure 10. SMOW—standard mean ocean water; VPDB—Vienna Peedee belemnite.

Calcite Concretions Containing Large, Iron-Oxide–Filled Rhombic Pseudomorphs or Iron-Oxide Accumulations along Cleavage Planes

At Egypt, Dry Fork, Buckskin Wash, Paria Canyon, and Three Lakes Canyon, many spheroidal calcite-cemented concretions are preferentially developed in the lower portions of grain-flow strata. Some spheroids are isolated (Fig. 7C), but others have merged into multiples, or have coalesced into large, slab-sided masses (Fig. 7A). Thin sections of the spheroids at Paria Canyon reveal porous, rhombic structures partially filled with iron oxide (Fig. 7D). At Dry Fork, white calcite-cemented concretions envelope many distinct iron-oxide–rich rhombs (Fig. 7E). These concretions are surrounded by a speckling of iron-rich masses that are identical in size to the rhombic structures within the concretions (Fig. 7F). Nielsen et al. (2009) showed that similar "speckles" are extremely common in the Navajo in Zion National Park. At Buckskin Wash, Paria Canyon, and Three Lakes Canyon, some concretionary masses are dominantly composed of coarse-grained calcite, but iron oxide is abundant along cleavage planes and former crystal faces. At Buckskin Wash, large concretionary masses cemented by ferroan calcite are abundant. The upper, weathered surfaces of some of these masses bear grooves with amplitudes up to one meter and wavelengths from 15 to 60 cm (Fig. 8A). In cross sections along canyon walls, calcite-cemented zones stand out in positive relief but show highly irregular boundaries (Fig. 8B). Resistant rock contains abundant, 6-mm-diameter, spheroidal concretions that are largely cemented by dark, ferroan calcite. The outer portions of these concretions are cemented by light-colored, iron-free calcite (Fig. 8B). The nonresistant rock contains iron-stained spheroids that are calcite free (Fig. 8C). The $\delta^{13}C$ values of calcite from Paria Canyon and Dry Fork range from –1.58‰ to –4.97‰ (Table 1).

Interpretation of Calcite Concretions Containing Large, Rhombic, Iron-Oxide Pseudomorphs or Iron-Oxide Accumulations along Cleavage Planes

These calcite concretions (Figs. 7A and 7C) aid interpretation of other concretions in the Navajo. The sizes and shapes of individual calcite spheroids are similar to those of the noncalcareous concretions with iron-oxide rinds (Fig. 2A) that we have interpreted as the remains

of former siderite concretions (Loope et al., 2010, 2011; Weber et al., 2012; this paper). The flat-topped, coalesced calcite concretions that develop in grain-flow strata have an overall form similar to some of the rinded boxworks (compare Figs. 7A and 7B).

Acid is generated by the hydrolysis that accompanies oxidation of Fe^{+2} to Fe^{+3} and subsequent precipitation of oxyhydroxides. Carbonate minerals with more than 50 mol% Fe are likely to be completely dissolved by a self-promoting oxidation reaction (Loope et al., 2010, p. 1002). Dissolution of carbonates with less iron consumes acid and is likely to lead to precipitation of iron-free calcite. We therefore interpret the cm-scale concretions at Dry Fork and Paria Canyon (Figs. 7C–7G) to have had <50 mol% Fe.

We interpret the "rhombic structures" within these concretions as pseudomorphs after either siderite (rhombs filled with iron oxide) or ankerite (rhombs retaining considerable pore space and partially filled by iron oxide). The "speckles" that lie outside the concretions (Fig. 7F) are the same size and general shape as those that are enclosed in calcite, but their margins are not as well defined. We interpret them as pseudomorphs after isolated iron-carbonate crystals.

The grooved surfaces and irregular shapes of sandstone masses at Buckskin Gulch that are cemented by ferroan calcite (Figs. 8A and 8B) could indicate large-scale amalgamation of cemented zones. Another possibility is that they indicate subsurface dissolution of ferroan calcite by acidic water. Acid could have been generated either during siderite oxidation or by dense, CO_2-charged water descending from the nearby Kaibab monocline. The iron-free rims on the small concretions (Fig. 8C) could be the result of a shift from reducing to oxidizing water or could have precipitated from oxidizing water as ferroan calcite underwent dissolution.

As with the calcite from Egypt, the high $\delta^{13}C$ values of the Dry Fork and Paria Canyon samples indicate that little of their carbon was derived from methane oxidation.

Iron-Oxide Patterns Preserved in Non-Calcareous Sandstone

At Zion Tunnel and Russell Gulch, iron-oxide cements form polygonal masses (mm scale) and patterns (cm scale). Some patterns comprise nested polygons defined by narrow bands of iron-oxide cement (Fig. 9). Scattered small masses produce a "speckled" appearance (Nielsen et al., 2009; Fig. 7E). These workers noted that most of the "speckles" are within their pink and their brown diagenetic facies but also occur in their white facies.

Interpretation of Iron-Oxide Patterns Preserved in Non-Calcareous Sandstone

As with the rinded concretions, we interpret these iron-oxide cements as the alteration products of precursor ferrous carbonates. Cross sections of many carbonate crystals are rhomb and hexagon shaped, and the carbonate crystals that grow in sandstones are very commonly large and poikilotopic (see Fig. 6B). We interpret the patterns defined by the polygons (Fig. 9) as the remains of poikilotopic carbonate euhedra—"sand crystals" that engulfed hundreds of sand grains. These euhedra contained both iron-rich and iron-poor zones. All of the carbonate in these crystals has been dissolved, leaving only iron oxide to mark the former positions of iron-rich zones. Acid generated during oxidation of the iron-rich zones (Loope et al., 2010) would have aided dissolution of the adjacent iron-poor calcite cement.

The "speckles" that Nielsen et al. (2009) described from Zion National Park are abundant in the Navajo in other parts of the Colorado Plateau and, based on their geometry and their resemblance to the pseudomorphs surrounding and within calcite concretions at Egypt and Dry Fork (Figs. 7E–7G), we interpret them as the oxidized remains of ferrous carbonate crystals. Nielsen et al. (2009, p. 73) noted that, at Zion, "speckles" are widespread within the bleached portions of the upper Navajo. With their mixing model for the primary (iron-oxide) origin of the speckles, it is necessary to reintroduce oxygenated waters below reducing water so that iron oxide can be emplaced as a primary phase in a previously bleached zone ("overprinting" of Nielsen et al., 2009). Our altered-precursor interpretation of these iron-oxide–cemented masses is consistent with their presence in bleached sandstone, because both bleaching of the sandstone (dissolution of iron oxide) and cementation by ferrous carbonates necessarily took place in reducing waters.

DISCUSSION

Carbon Dioxide Giants or Broad Flow Paths?

Using satellite imagery and field-based spectral reflectance measurements, Beitler et al. (2003, 2005) argued that the bleached sand-

Figure 7 (*on following page*). Carbonate and iron-oxide cements and concretions. (A) Wedge-shaped toes of eolian grain flows (GF; site E, Fig. 1) are preferentially cemented by ferroan calcite and surrounded by uncemented wind-ripple deposits (wr). White arrows point to planar, upper surface of cemented wedge—the former avalanche face of an eolian dune. Cementation began with spheroidal concretions and ended with slab-sided masses. (B) Boxwork concretion (iron oxide, no preserved carbonates; site CC, Fig. 1) that is bounded by a thick iron-oxide rind with a planar, upper surface (white arrows; top of grain-flow stratum). Internal compartments are defined by iron oxide that precipitated along two perpendicular sets of joints (J). Two cores (c) occupy the centers of the two visible compartments. Interpretation: Siderite preferentially developed in grain-flow strata (as did calcite in A); upon oxidation, the iron-oxide rind followed the original grain flow–wind-ripple boundary (the upper edge of the former, siderite-cemented mass). (C) Oblate-spheroidal concretions in wind-ripple deposits at Paria Canyon (PC; Fig. 1). (D) Plane-light micrograph from a concretion (as in C and E). Calcite (c) is preserved, but the rhombic, iron-rich areas (white arrows) are pseudomorphs of an iron-rich carbonate phase (probably ankerite) that was originally in optical continuity with the calcite but was dissolved, leaving iron oxide (black) and pore space (blue). These rhombs resemble those seen dispersed in sandstones that lack calcite cement—the "speckles" of Nielsen et al. (2009) and in the core stones shown in Figure 2. (E) Sawn halves of a single calcite-cemented concretion from Paria Canyon (as in C and D). Black arrow points to a central, rhomb-shaped, iron-rich zone. White arrows point to a thin, rhomb-shaped, iron-oxide–rich zone that defines the perimeter of a large, heavily altered carbonate crystal. Interpretation: Two zones (with the same poikilotopic crystal) that were originally composed of siderite or ankerite dissolved in oxidizing pore water, leaving iron oxide to mark their former positions. Small, dark structures are pseudomorphs (ps) also shown in D and G. (F) Sandstone exposed at Dry Fork with isolated, dark speckles (S) and large concretions with dense, calcite-cemented cores (black arrows) and perimeters composed of closely spaced speckles (white arrows). (G) Sawed sections of the large white cores of concretions shown in (F). The dense, calcite-cemented sandstone contains numerous scattered, 3- to 4-mm-diameter, iron-oxide masses (black arrows) interpreted as pseudomorphs after iron-rich carbonate crystals. These closely resemble the iron-rich areas shown in D and the "speckles" shown in F; all are interpreted as rhombic pseudomorphs after siderite or ankerite.

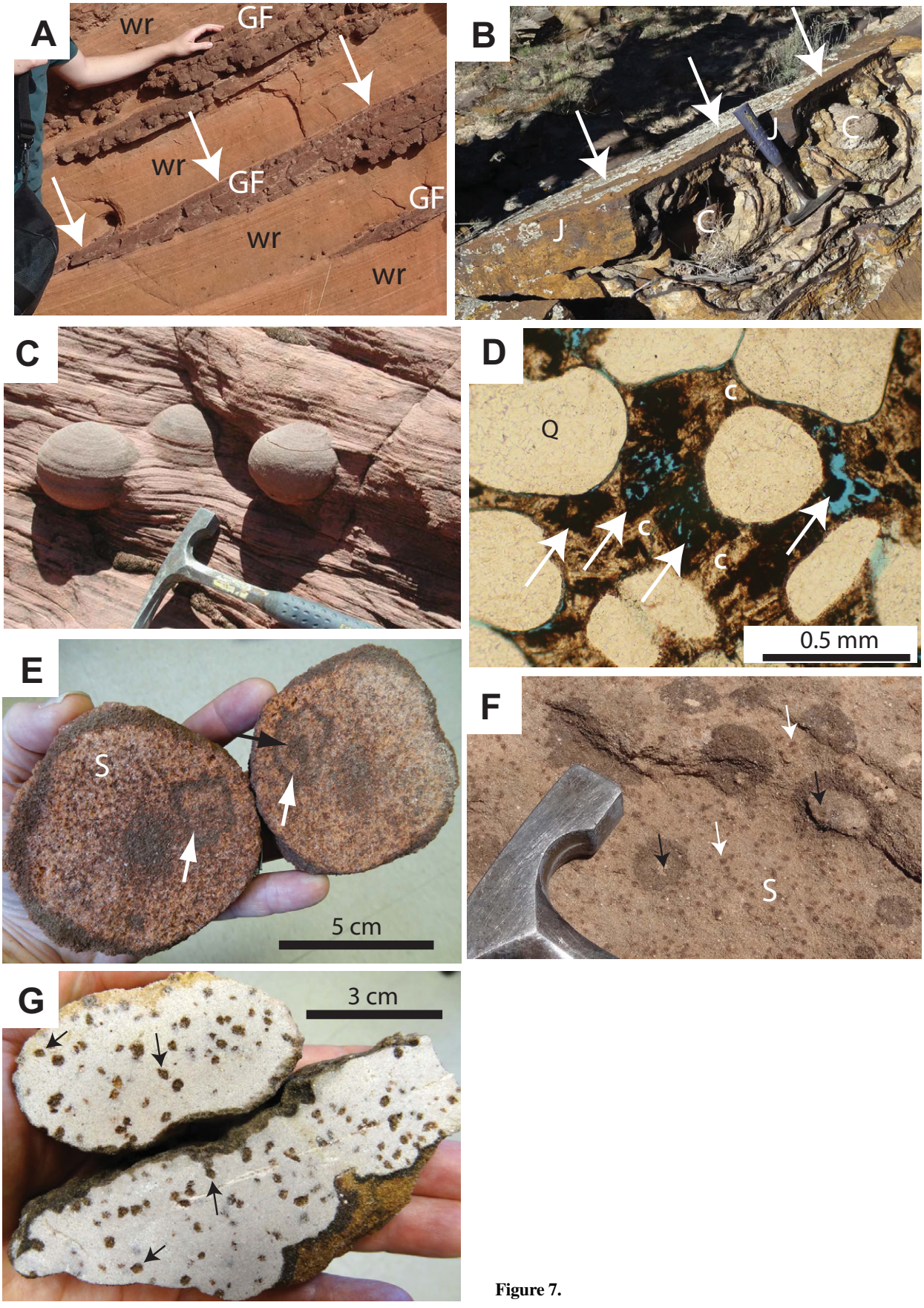

Figure 7.

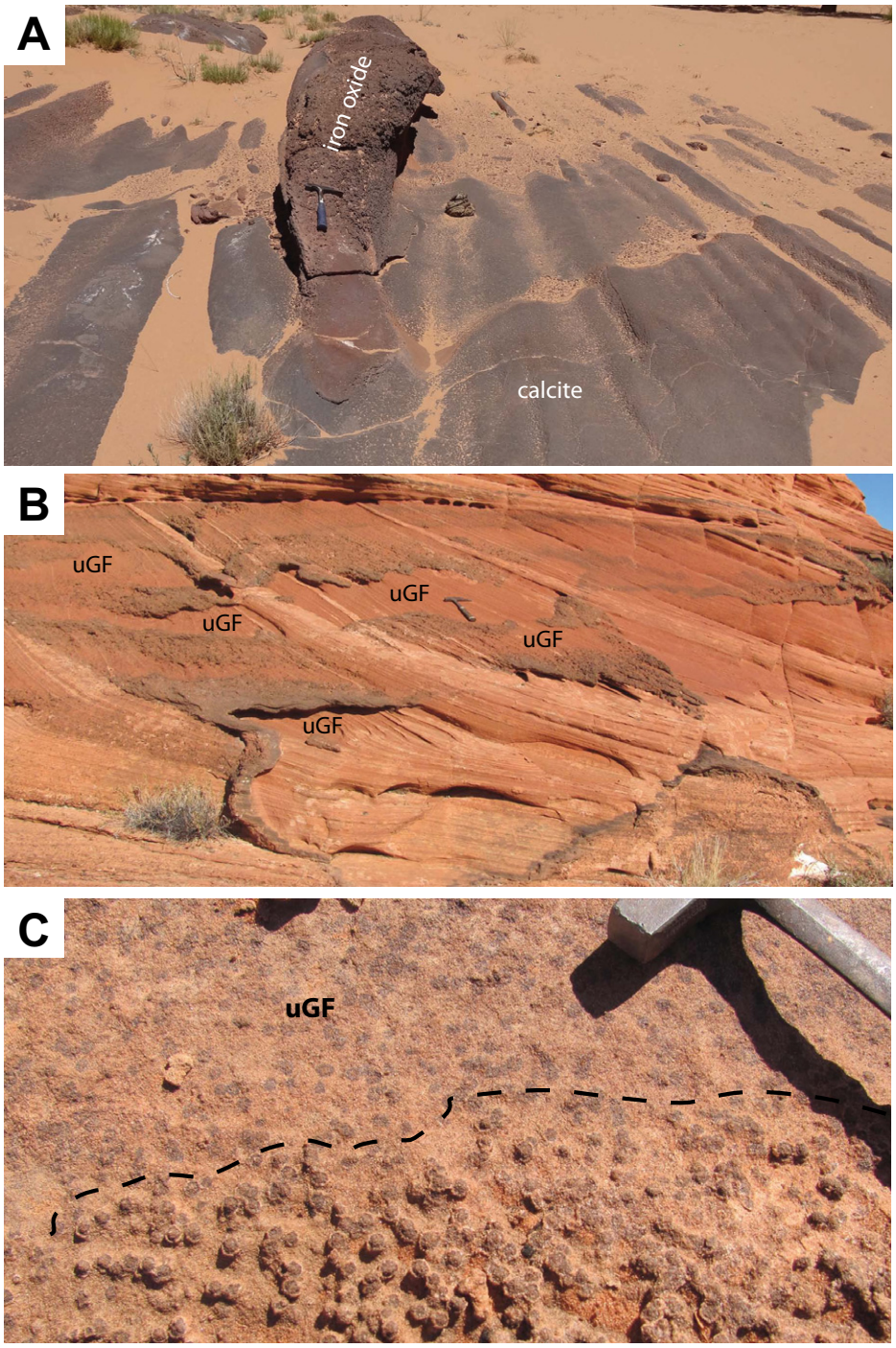

Figure 8. Possible evidence for subsurface dissolution of late diagenetic cement composed of ferroan calcite. (A) Upper surface of a broad mass of calcite- and iron-oxide–cemented sandstone. (B) Irregular distribution of ferroan calcite cement in Navajo cross strata. Grain-flow strata are preferentially cemented, but large, irregular patches of uncemented grain flows (uGF) suggest that some cements have been dissolved. (C) Boundary between cemented (below dashed line) and uncemented grain flows. Small spheroids within uGFs are not calcareous and are stained by iron oxide. Note the thin rims of light-colored, iron-poor calcite on each ferroan-calcite–cemented spheroid below the dashed line.

stones across many of the Colorado Plateau anticlines mark the positions of "exhumed hydrocarbon giants." No bitumen, however, has been reported from bleached Navajo Sandstone, and only a very small quantity of bitumen is present in the Entrada Sandstone (at one site). We interpret the $\delta^{13}C$ values (Fig. 10) of the carbonates associated with the bleached rocks as evidence that a portion of the carbon was derived from organic sources. This evidence, combined with the widespread surviving and altered carbonate concretions, leads us to agree with Haszeldine et al. (2005) that bleaching was accomplished via large volumes of carbon dioxide and a lesser amount of methane.

Wigley et al. (2012) studied bleached Entrada Sandstone and carbonate cements associated with active CO_2 seeps along a fault near the crest of an anticline at Green River, Utah. They concluded that the Entrada was bleached by an aqueous solution in which carbon was predominantly oxidized (CO_2; 93%), with lesser amounts of methane (7%):

$$20Fe_2O_{3(\text{hematite})} + 5CH_{4(aq)} + 64CO_{2(aq)} + 19H_2O + 11H^+_{(aq)} = 30Fe^{2+}_{(aq)} + 10FeHCO^+_{3(aq)} + 59HCO^-_{3(aq)}. \quad (1)$$

The $\delta^{13}C$ values from cement samples at Green River (Wigley et al., 2012) were only slightly heavier than those reported by Beitler et al. (2005). Because our $\delta^{13}C$ values (mean of –3.12‰), are very near those reported by Wigley et al. (2012), they, too, are more consistent with bleaching by a fluid carrying mostly inorganic carbon.

Nielsen et al. (2009) emphasized that the bleaching of the upper Navajo could not have taken place under static conditions—sustained fluid flow was necessary to strip iron oxide from sand grains. Furthermore, Parry (2011) showed that, because of the low solubility of ferrous iron, the growth of iron-rich concretions in the Navajo Sandstone required advective flow through the aquifer for thousands of years. We propose that, over a large portion of our study area, two linked, density-driven flow systems operated to bleach the sandstone and to transport sufficient iron to precipitate the concretions: (1) buoyant up-dip flow of methane and supercritical carbon dioxide; and (2) convective flow driven by the enhanced density of waters carrying aqueous CO_2 in contact with overlying, migrating or trapped supercritical CO_2 (Fig. 11). Dissolution can yield a solution that is ~5 wt% CO_2; Bickle (2009) notes that if the reservoir has high permeability, a 50-m-thick layer of CO_2 can be dissolved in ten years. Upslope migration continually exposes migrating CO_2 to unsaturated waters, making dissolution more

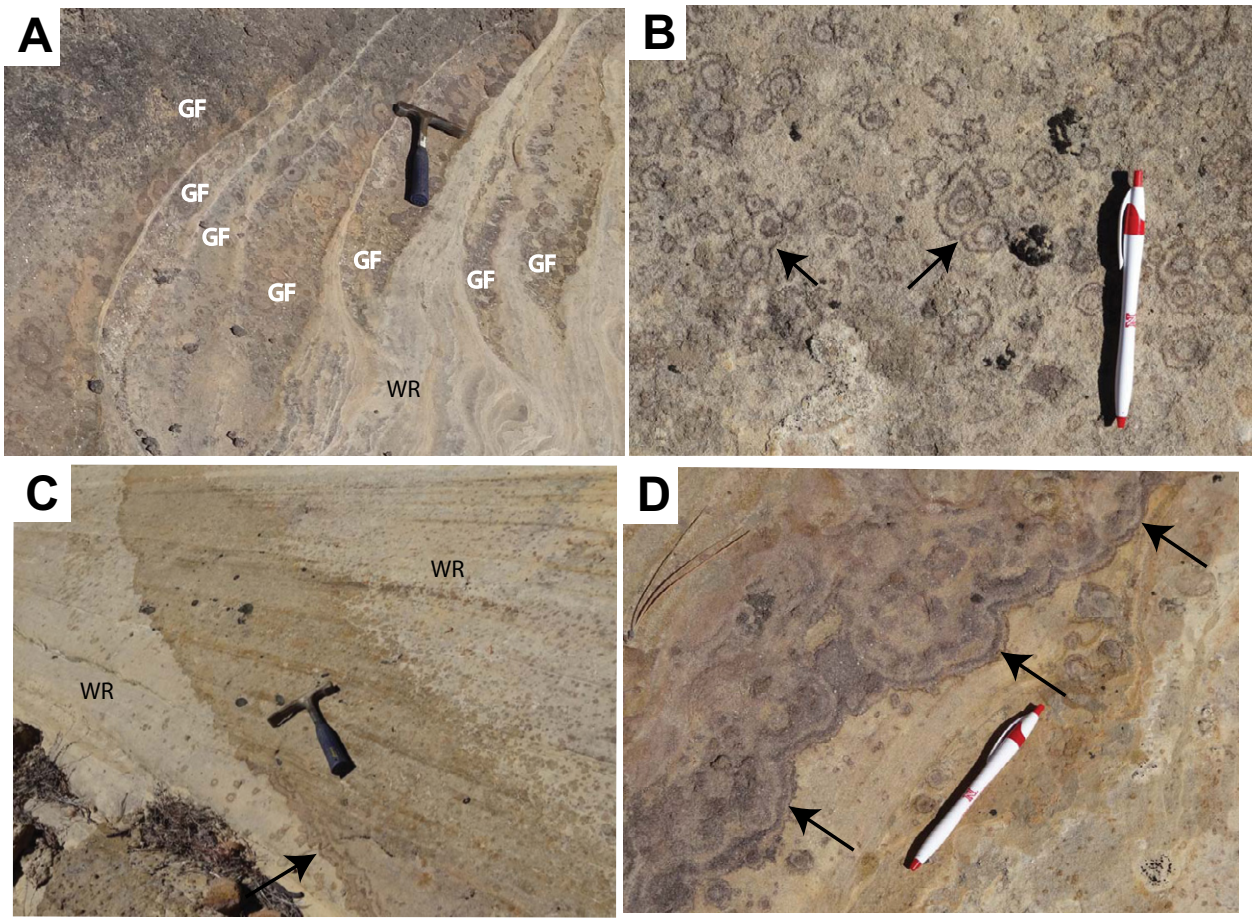

Figure 9. Patterned iron-oxide cements in non-calcareous sandstone (site RG, Fig.1). (A) Grain-flow (GF) tongues preferentially cemented by iron oxide (cf. Fig. 7A). (B) Close-up grain flow (as in A) with nested polygonal patterns defined by iron-oxide bands. Arrowed bands surround multiple pattern elements. Interpretation: Iron-oxide bands are the oxidized and dissolved remains of large, iron-zoned, euhedral carbonate crystals. (C) Large swath of iron-oxide stain that cuts across wind-ripple crossbedding in the white subfacies of the Navajo Sandstone. Upper margin of swath grades into patterned iron oxide as shown in B and "speckles" (Figs. 7E–7G). Lower margin (arrow) contains distinct, dark iron-oxide bands. (D) Close-up of band arrowed in C. Interpretation: The dark, continuous band (arrows) is the oxidized and dissolved remnant of an iron-rich zone that grew within sandstone that was densely cemented by carbonate minerals with varying iron content. WR—wind-ripple deposits.

efficient; descent of the density-enhanced water (charged with aqueous CO_2) can arrest the upslope flow of the buoyant fluid (MacMinn and Juanes, 2013; Fig. 11). The great extent and relatively uniform thickness of the bleached rock on the Colorado Plateau (e.g., the White Cliffs, Fig. 1) reflect the interaction of these two flow systems. The low northward dip of the Navajo Sandstone along the east-west–oriented White Cliffs of southwestern Utah (Fig. 1) suggests that CO_2 migrated southward toward a broad, now eroded structural high. The abundance of concretions along the east flank of the Kaibab upwarp indicates that CO_2 very likely accumulated along the crest of that structure. Rather than developing only within or immediately below giant CO_2 reservoirs, however, a large

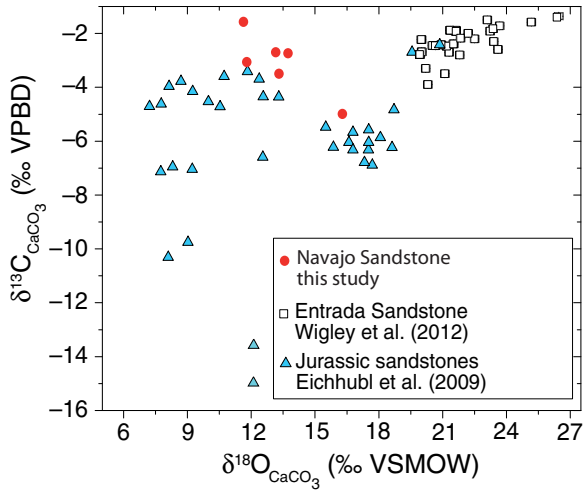

Figure 10. Plot of carbon and oxygen isotopes for calcite cements and concretions from the Egypt, Dry Fork, and Paria Canyon localities (red dots; see Table 1) and comparison with values from other sandstones in the region. Triangles mark values from Chan et al. (2000), Eichhubel (2009), and Garden et al. (2001. Modified from Wigley et al. (2012). VPDB—Vienna Pee Dee belemnite; VSMOW—Vienna standard mean ocean water.

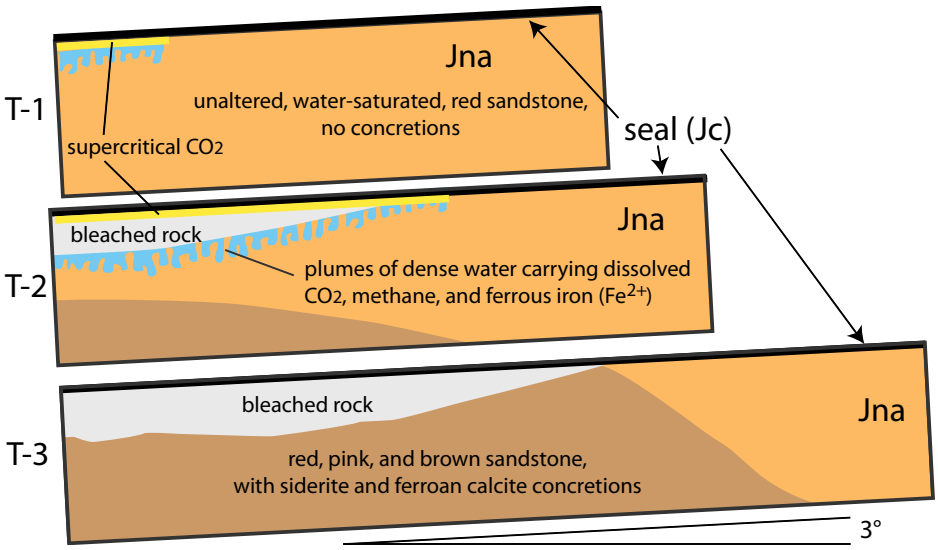

Figure 11. Model for bleaching of upper Navajo Sandstone and precipitation of ferrous concretions in the middle Navajo. T-1: Moving up dip, just below the sealing Carmel Formation, buoyant, supercritical carbon dioxide and a small quantity of methane starts to accumulate in the upper Navajo Sandstone. Dissolution of CO_2 into underlying water begins. T-2: Supercritical carbon dioxide in contact with underlying formation water continues to move up dip and to dissolve. As aqueous carbon dioxide adds mass to the solution, the dense fluid moves downward as finger flow. Methane reduces hematite on the rims of sand grains, releasing ferrous iron into solution and bleaching the rock. The descending water transports ferrous iron and remaining methane downward. T-3: Carbon dioxide is depleted, and downward flow has ceased. Siderite and ferroan calcite have precipitated in the middle Navajo (perhaps facilitated by localized degassing of carbon dioxide). Up-dip extent of bleached rock marks limit of CO_2 migration, a possible explanation for the presence of unbleached sandstone in northernmost Zion National Park (noted by Nielsen et al., 2009). Final thickness of bleached zone reflects quantity of methane available for reduction of ferric iron during descent of plumes. Modified from MacMinn and Juanes (2013, fig. 1). Jna—Jurassic Navajo Sandstone; Jc—Jurassic Carmel Formation.

proportion of the bleached rocks and carbonate concretions most likely developed along gently sloping flow paths along which the CO_2 and methane never reached a structural trap (the dense water descended before reaching a trap or the ancient land surface; Fig. 11).

Hydrodynamic flow may have also played a role in the bleaching and emplacement of concretions. The positions of the Escalante anticline and the Aquarius Plateau were suitable for hydrodynamic flow through the Navajo Sandstone during portions of the middle and late Cenozoic (Loope et al., 2010). A sister anticline just west of the Escalante structure (the Upper Valley anticline) presently has hydrodynamic flow from the Aquarius Plateau (Allin, 1993).

Sequence of Events and Their Relationships to Landform Evolution

Clarence Dutton's (1882) "Great Denudation" was a long erosive episode during which Mesozoic strata were stripped northward from the Grand Canyon, thereby generating southern Utah's Grand Staircase. To bleach the upper Navajo across the crest of the Kaibab upwarp from the west of the Hurricane fault to the Kaibab monocline—a distance of 110 km—required a continuous, confined aquifer. Bleaching the upper Navajo, precipitating ferrous carbonates, and oxidizing those carbonates required the following sequence of geologic events: (1) compressive stresses tilted reservoir and sealing rocks into broad folds; (2) methane from thermally mature strata migrated northward along with supercritical CO_2 released from magma; (3) waters with enhanced density flowed downward from the base of migrating or trapped supercritical CO_2; (4) extensional stresses produced normal faults and fractures that allowed degassing of CO_2, facilitating nucleation and growth of ferrous carbonate concretions and cements; (5) thermal expansion during continuing uplift generated numerous, closely spaced joints (Fossen, 2010); and (6) dissection of the Colorado Plateau led to flushing of reducing water by oxygenated meteoric water, oxidation of iron-rich carbonates, and drainage of much of the Navajo aquifer.

After they were eroded during latest Cretaceous and early Paleogene time, tilted Cretaceous rocks along the Kaibab monocline were buried by flat-lying, Middle Eocene lacustrine sediment (ca. 40 Ma; Eaton et al., 2011; Dickinson et al., 2012). The Navajo aquifer was intact at this stage; its highest elevation (crest of the Kaibab Plateau) would have approximated that of the Eocene lake beds. Post-uplift, those beds crop out along the southern edge of Aquarius Plateau, just east of the Paunsaugunt fault (Fig. 1; presently ~3100 m). Oligocene volcanics started to erupt at 32 Ma and buried the lake beds. After release of supercritical CO_2 from intrusive magma and its migration into the Navajo, dissolution of carbon dioxide into the pore waters immediately below the supercritical CO_2 slowed or stopped its buoyant, up-dip migration (MacMinn and Juanes, 2013; Fig. 11). Methane dissolved in the water bleached the upper Navajo and, as $CO_{2(aq)}$ accumulated, the fluid moved downward, transporting ferrous iron and remaining methane into lower strata. As extensional faulting started to break up the western Colorado Plateau (12–15 Ma; Davis, 1999), degassing adjacent to joints would have increased alkalinity of the water, thereby triggering precipitation of carbonate minerals. Eventually, block faulting ruptured and offset the seal formed at the top of the Navajo, releasing the buoyant fluids and ending convective flow within the Navajo aquifer.

Recently published (U-Th)/He ages of Colorado Plateau iron-oxide accumulations indicate they precipitated between 0.21 and 25 Ma (Reiners et al., 2014). These are likely oxidation ages—helium accumulation had to wait until after precursor siderite was altered to iron oxide. Entry of oxygenated, meteoric water into the Navajo initiated rind-forming, microbial oxidation of siderite. Collapse in the Basin and Range led to headward erosion and deep dissection of Plateau strata. Lucchitta et al. (2011) made a strong case that a river flowing southwestward from Colorado was coursing through the Kaibab upwarp in what is now eastern Grand Canyon by the Middle Miocene. Karlstrom et al. (2014) calculated that, by 6 Ma, the river crossing the Kaibab upwarp had already incised all Mesozoic strata and had reached the Mississippian Redwall Limestone. From these interpretations, we conclude that density-driven, convective flow within the Navajo aquifer started ca. 30 Ma (strata had been tilted and CO_2 delivery initiated). Precipitation of ferrous carbonates probably ended across most of the study area between 15 and 6 Ma (breach of sealing strata and influx of oxygen-

ated, meteoric water). Ongoing uplift of the Colorado Plateau ensures that cooling will continue to generate new, closely spaced joints and that meteoric water will displace reducing waters remaining in structurally lower parts of the Navajo, and any siderite surviving there will be oxidized.

Concretion Morphology and Timing of Aquifer Drainage

The Lava Point basalt flow in west-central Zion National Park (dated at 1.02 ± 0.02 Ma) followed paleodrainages cut into the Navajo Sandstone (Biek et al., 2003). Due to its resistance to erosion, this rock now caps mesas that stand 400 m above the Virgin River and its tributary canyons (Fig. 12; Biek et al., 2003). Rinded concretions with central cores (including both small spheroids and large ironstone masses) are abundant in Navajo outcrops that are laterally adjacent to and 30–150 m below the base of the Lava Point flow (Figs. 2A, 3A, and 12). "Comet tails" (Fig. 4A) extend southwestward from the small spheroids. These relationships suggest an explanation for why rind formation goes to completion in some concretions but is incomplete in others (the concretions that retain central cores; Fig. 5): Rinds were forming on sideritic concretions at ca. 1 Ma—a time when they lay within oxidizing, southwest-flowing groundwater, a few tens of meters below the water table. Post-lava incision of Russell Gulch lowered the water table below the oxidizing concretions (Fig. 12). Rind formation then ceased, and any remaining siderite in these concretions was oxidized abiotically in the vadose zone.

CONCLUSIONS

Bleaching of the upper Navajo Sandstone along the White Cliffs and precipitation of iron-rich concretions of the same formation in the Vermillion Cliffs took place in a vertically confined, near-horizontal aquifer in which two flow systems interacted. Buoyant fluids (supercritical carbon dioxide sourced from Oligocene–Miocene intrusions and small amounts of methane) moved up dip along the sealing strata

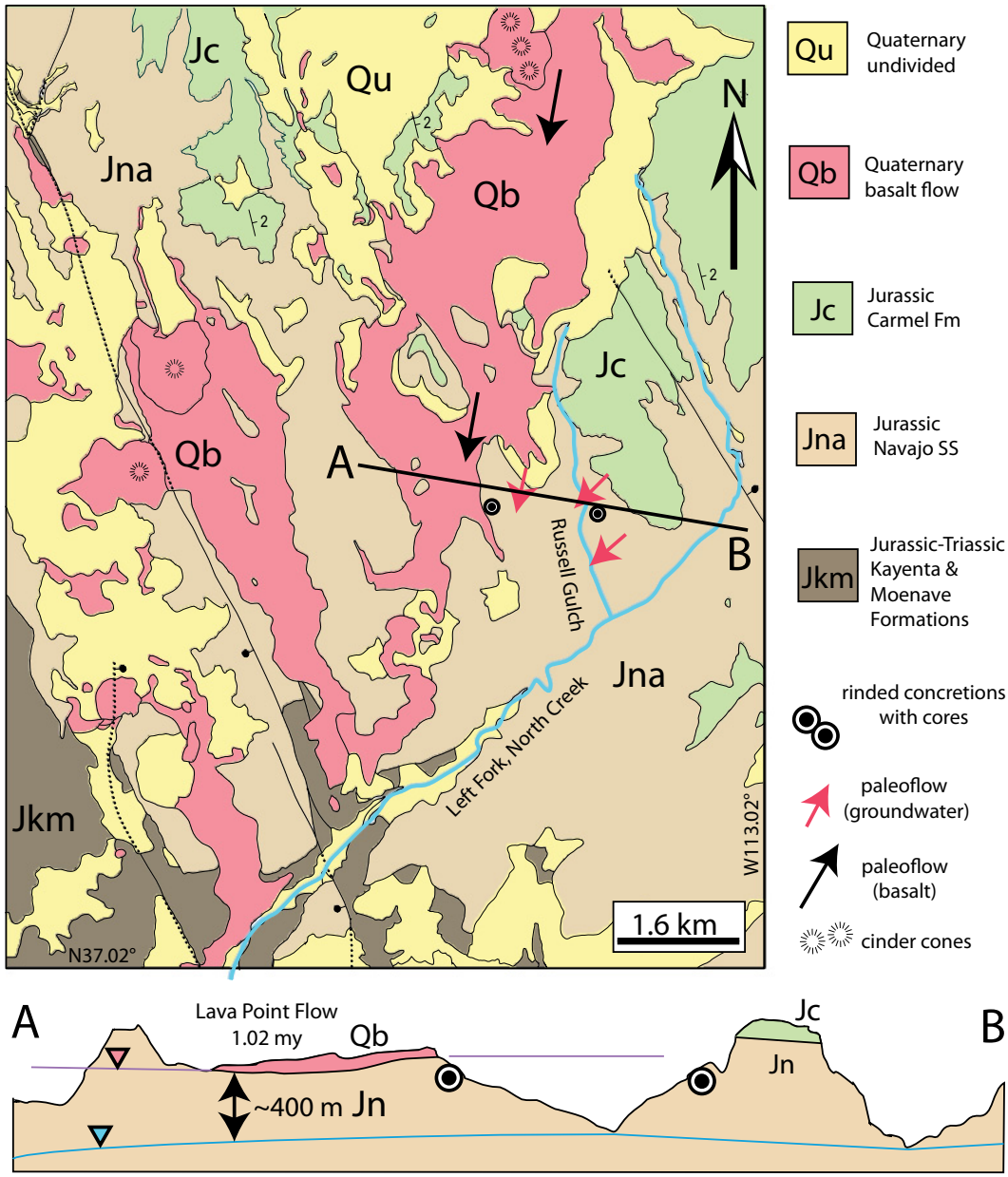

Figure 12. Map and cross section showing distribution (within central Zion National Park; Site RG, Fig. 1) of Late Pleistocene basalt, Navajo Sandstone, capping strata of the Carmel Formation, and rinded concretions with central cores (see Figs. 2 and 3A). Basalt flowed down the paleovalley of North Creek (a tributary of the Virgin River) that was cut into the Navajo Sandstone (Biek et al., 2003). Modern canyon floors of North Creek, Russell Gulch, and the Virgin River are ~400 m lower than the base of the basalt. Triangles mark approximate positions of ancient (upper) and modern groundwater tables. Cores of concretions record timing of water-table fall below level of concretions. This halted the cm-scale diffusion of water that is necessary for continued thickening of the rinds. Cores were then oxidized abiotically (Fig. 5). Flow direction of groundwater (red arrows) was discerned from concretions (Fig. 4). Note near parallelism of groundwater flow direction, flow direction of basalt, and flow direction of North Creek. Modified from Interactive Geologic Map of Utah (http://geology.utah.gov/map/geomap/interactive/viewer).

of the Carmel Formation and bleached the upper Navajo. As CO_2 dissolved into the underlying water, the added density caused that solution to sink down section, carrying ferrous iron and methane with it. Upon loss of CO_2 along joints, siderite and ferroan calcite concretions precipitated, sequestering copious carbon in the middle Navajo. Siderite is now absent from Navajo outcrops, but the ferrous iron and carbon isotopes in the preserved calcite concretions are independent testimony to the presence of reducing, CO_2-charged pore water. Post-Miocene uplift of the Colorado Plateau and collapse of the Basin and Range Province led to canyon cutting and drainage of pore water from the Navajo Sandstone. Thermal contraction during uplift led to proliferation of closely spaced joints that fractured many of the large siderite concretions and became conduits for fluid flow. When oxygenated meteoric water reached the siderite concretions, it altered them into rinded, iron-oxide concretions. Many of the large concretions retain central cores with iron-oxide pseudomorphs after siderite. Cored, pseudomorph-bearing concretions that lie below valley-filling, Late Pleistocene lava flows strongly suggest that much of the siderite was oxidized very recently (<1 Ma)—a conclusion consistent with some of the recently reported (U-Th)/He ages from Navajo Sandstone concretions (Reiners et al., 2014). When the concretions emerged above the water table, the cm-scale diffusion needed for rind formation was no longer possible. The siderite remaining in concretion cores was therefore oxidized in the vadose zone, preserving the pseudomorphs. These relationships make it likely that some siderite remains in the subsurface and that oxidation continues in some areas. Further absolute dating of different portions of these concretions could test the ideas presented here and could reveal uplift rates for a large portion of the Colorado Plateau. Bleached sandstones, iron-oxide–cemented concretions, and ferroan calcite concretions in other strata may reveal flow systems with similar configurations and histories.

ACKNOWLEDGMENTS

We greatly appreciate the helpful reviews by Peter Mozley and Laura Crossey. We also thank Jim Elder, Jon Mason, Jodi Norris, and Shirley Yik for help during fieldwork and Andrew Hutsky and Tracy Frank for help with isotopes. Kevin Miller and Carolyn Shelton (Grand Staircase–Escalante National Monument) and Kezia Nielsen and Jock Whitworth (Zion National Park) provided encouragement and logistical assistance.

REFERENCES CITED

Allin, D.L., 1993, Upper Valley, *in* Hill, B.G., and Bereskin, S.R., eds., Oil and Gas Fields of Utah: Utah Geological Association Publication 22, 192 p.

Barge, L.M., Hammond, D.E., Chan, M.A., Potter, S., Petruska, J., and Nealson, K.H., 2011, Precipitation patterns formed by self-organizing processes in porous media: Geofluids, v. 11, p. 124–133, doi:10.1111/j.1468-8123.2010.00324.x.

Bickle, M.J., 2009, Geological carbon storage: Nature Geoscience, v. 2, p. 815–818.

Beitler, B., Chan, M.A., and Parry, W.T., 2003, Bleaching of Jurassic Navajo Sandstone on Colorado Plateau Laramide highs: Evidence of exhumed hydrocarbon supergiants?: Geology, v. 31, p. 1041–1044.

Beitler, B., Parry, W.T., and Chan, M.A., 2005, Fingerprints of fluid flow: Chemical diagenetic history of the Jurassic Navajo Sandstone, southern Utah, U.S.A: Journal of Sedimentary Research, v. 75, p. 547–561, doi:10.2110/jsr.2005.045.

Biek, R.F., Willis, G.C., Hylland, M.D., and Doelling, H.H., 2003, Geology of Zion National Park, Utah, *in* Sprinkel, D.A., Chidsey, T.C., and Anderson, P.B., eds., Geology of Utah's Parks and Monuments: Utah Geological Association Publication 28, p. 107–135.

Bowers, W.E., 1991, Geologic map of Bryce Canyon National Park and vicinity, southwestern Utah: U.S. Geological Survey Miscellaneous Investigations Series Map I-2108, scale 1:24,000.

Burnside, N.M., Shipton, Z.K., Dockrill, B., and Elam, R.M., 2013, Man-made versus natural CO_2 leakage: A 400 k.y. history of an analogue for engineered geological storage of CO_2: Geology, v. 41, p. 471–474.

Busigny, V., and Dauphas, N., 2007, Tracing paleofluid circulations using iron isotopes: A study of hematite and goethite concretions from the Navajo Sandstone (Utah, USA): Earth and Planetary Science Letters, v. 254, p. 272–287, doi:10.1016/j.epsl.2006.11.038.

Chan, M.A., Parry, W.T., and Bowman, J.R., 2000, Diagenetic hematite and manganese oxides and fault-related fluid flow in Jurassic Sandstones of southeastern Utah: American Association of Petroleum Geologists Bulletin, v. 84, p. 1281–1310.

Chan, M.A., Bowen, B.B., and Parry, W.T., 2005, Red rock and red planet diagenesis: Comparisons of Earth and Mars concretions: GSA Today, v. 15, no. 8, doi:10.1130/1052–5173(2005) 015<4:RRARPD>2.0.CO;2.

Chan, M.A., Johnson, C.M., Beard, B.L., Bowman, J.R., and Parry, W.T., 2006, Iron isotopes constrain the pathways and formation mechanisms of terrestrial oxide concretions: A tool for tracing iron cycling on Mars?: Geosphere, v. 2, p. 324–332, doi:10.1130/GES00051.1.

Chan, M.A., Ormo, J., Park, M., Stich, M., Souza-Egipsy, V., and Komatsu, G., 2007, Models of iron oxide concretion formation: field, numerical, and laboratory comparisons: Geofluids, v. 7, p. 356–368, doi:10.1111/j.1468-8123.2007.00187.x.

Crossey, L.J., Fischer, T.P., Patchett, P.J., Karlstrom, K.E., Hilton, D.R., Newell, D.L., Huntoon, P., Reynolds, A.C., and de Leeuw, G.A.M., 2006, Dissected hydrologic system at the Grand Canyon: Interaction between deeply derived fluids and plateau aquifer waters in modern springs and travertine: Geology, v. 34, p. 25–28, doi:10.1130/G22057.1.

Crossey, L.J., Karlstrom, K.E., Springer, A.E., Newell, D., Hilton, D.R., and Fischer, T., 2009, Degassing of mantle-derived CO_2 and He from springs in the southern Colorado Plateau region—Neotectonic connections and implications for groundwater systems: Geological Society of America Bulletin, v. 121, p. 1034–1053, doi:10.1130/B26394.1.

Crow, R., Karlstrom, K.E., McIntosh, W., Peters, L., and Dunbar, N., 2008, History of Quaternary volcanism and lava dams in western Grand Canyon based on lidar analysis, $^{40}Ar/^{39}Ar$ dating, and field studies: Implications for flow stratigraphy, timing of volcanic events, and lava dams: Geosphere, v. 4, p. 183–206, doi:10.1130/GES00133.1.

Davis, G.H., 1999, Structural Geology of the Colorado Plateau Region of Southern Utah: Geological Society of America Special Paper 342, 157 p.

Dickinson, W.R., Lawton, T.F., Pecha, M., Davis, S.J., Gehrels, G.E., and Young, R.A., 2012, Provenance of the Paleogene Colton Formation (Uinta Basin) and Cretaceous–Paleogene provenances evolution in the Utah foreland: Evidence from U-Pb ages of detrital zircons, paleocurrent trends, and sandstone petrofacies: Geosphere, v. 8, no. 4, p. 854–880, doi:10.1130/GES00763.1.

Dutton, C.E., 1882, Tertiary History of the Grand Canyon with Altas: U.S. Geological Survey, Government Printing Office, 264 p.

Eaton, J.G., Tibert, N.E., and Biek, R.F., 2011, First mammals and ostracodes from the Paleogene Claron Formation, southwestern Utah: Geological Society of America Abstracts with Programs, v. 43, no. 4, p. 77.

Eichhubl, P., Davatzes, N.C., and Becker, S.P., 2009, Structural and diagenetic control of fluid migration and cementation along the Moab Fault, Utah: American Association of Petroleum Geologists Bulletin, v. 93, p. 653–681.

Ennis-King, J., and Paterson, L., 2005, Role of convective mixing in the long-term storage of carbon dioxide in deep, saline aquifers: Society of Petroleum Engineers Journal, v. 10, no. 3, p. 349–356.

Fossen, H., 2007, Deformation bands in sandstone: A review: Journal of the Geological Society, London, v. 164, p. 755–769, doi:10.1144/0016-76492006-036.

Fossen, H., 2010, Structural Geology: Cambridge, Cambridge University Press, 463 p. (p. 86–88; 137, 147).

Garden, I.R., Guscott, S.C., Burley, S.D., Foxford, K.A., Walsh, J.J., and Marshall, J., 2001, An exhumed palaeo-hydrocarbon migration fairway in a faulted carrier system, Entrada Sandstone of SE Utah, USA: Geofluids, v. 1, p. 195–213, doi:10.1046/j.1468-8123.2001.00018.x.

Gilfillan, S.M.V., Ballentine, C.J., Holland, G., Blagburn, D., Lollar, B.S., Stevens, S., Schoell, M., and Cassidy, M., 2008, The noble gas geochemistry of natural CO_2 gas reservoirs from the Colorado Plateau and Rocky Mountain provinces, USA: Geochimica et Cosmochimica Acta, v. 72, p. 1174–1198, doi:10.1016/j.gca.2007.10.009.

Hamblin, W.K., 1970, Late Cenozoic basalt flows of the western Grand Canyon, *in* Hamblin, W.K., and Best, M.G., eds., The Western Grand Canyon District: Utah Geological Society Guidebook to the Geology of Utah, no. 23, p. 21–38.

Haszeldine, R.S., Quinn, O., England, G., Wilkinson, M., Shipton, Z.K., Evans, J.P., Heath, J., Crossey, L., Ballentine, C.J., and Graham, C.M., 2005, Natural geochemical analogues for carbon dioxide storage in deep geological porous reservoirs, a United Kingdom perspective: Oil & Gas Science and Technology, v. 60, p. 33–49, doi:10.2516/ogst:2005004.

Heath, J.E., Lachmar, T.E., Evans, J.P., Kolesar, P.T., and Williams, A.P., 2009, Hydrogeochemical characterization of leaking carbon-dioxide-charged fault zones in east-central Utah, with implications for geologic carbon storage, *in* McPherson, B.J., and Sundquist, E.T., eds., Carbon Sequestration and Its Role in the Global Carbon Cycle: Geophysical Monograph Series, v. 183, p. 147–158.

Kampman, N., Bickle, M., Wigley, M., and Dubacq, B., 2014, Fluid flow and CO_2-fluid-mineral interactions during CO_2-storage in sedimentary basins: Chemical Geology, v. 369, p. 22–50, doi:10.1016/j.chemgeo.2013.11.012.

Karlstrom, K.E., Crow, R.S., Peters, L., McIntosh, W., Raucci, J., Crossey, L.J., Umhoefer, P., and Dunbar, N., 2007, $^{40}Ar/^{39}Ar$ and field studies of Quaternary basalts in Grand Canyon and model for carving Grand Canyon: Quantifying the interaction of river incision and normal faulting across the western edge of the Colorado Plateau: Geological Society of America Bulletin, v. 119, p. 1283–1312, doi:10.1130/0016-7606(2007)119[1283:AAFSOQ]2.0.CO;2.

Karlstrom, K.E., Coblentz, D., Dueker, K., Ouimet, W., Kirby, E., Van Wijk, J., Schmandt, B., Kelley, S., Lazear, G., Crossey, L.J., Crow, R., Aslan, A., Darling, A., Aster, R., MacCarthy, J., Hansen, S.M., Stachnik, J., Stockli, D.F., Garcia, R.V., Hoffman, M., Keon, R., Feldman, J., Helzer, M., and Donahue, M.S., and the CREST Working Group, 2012, Mantle-driven dynamic uplift of the Rocky Mountains and Colorado Plateau and its surface response: Toward a unified hypothesis: Lithosphere, v. 4, p. 3–22, doi:10.1130/L150.1.

Karlstrom, K.E., Lee, J.P., Kelley, S.A., Crow, R.S., Crossey, L.J., Young, R.A., Lazear, G., Beard, L.S., Ricketts, J.W., Fox, M., and Shuster, D.L., 2014, Formation of the Grand Canyon 5 to 6 million years ago via integration of older palaeocanyons: Nature Geoscience, v. 7, p. 239–244, doi:10.1038/ngeo2065.

Kettler, R.M., Loope, D.B., and Weber, K.A., 2011, Follow the water: Connecting a CO_2 reservoir and bleached sandstone to iron-rich concretions in the Navajo Sandstone of south-central Utah, USA: REPLY: Geology, v. 39, no. 11, p. e251–e252, doi:10.1130/G32550Y.1.

Kocurek, G., and Dott, R.H., Jr., 1983, Jurassic paleogeography and paleoclimate of the central and southern Rocky Mountains regions, *in* Reynolds, M.W., and Dolly, E.D., eds., Mesozoic Paleogeography of the West-Central United States: Rocky Mountain Section, SEPM (Society for Sedimentary Geology), p.101–116.

Lindeberg, E., and Wessel-Burg, D., 1997, Vertical convection in an aquifer column under a gas cap of CO_2: Energy Conversion and Management, v. 38, p. S229–S234, doi:10.1016/S0196-8904(96)00274-9.

Loope, D.B., Kettler, R.M., and Weber, K.A., 2010, Follow the water: Connecting a CO_2 reservoir and bleached sandstone to iron-rich concretions in the Navajo Sandstone of south-central Utah, USA: Geology, v. 38, p. 999–1002, doi:10.1130/G31213.1.

Loope, D.B., Kettler, R.M., and Weber, K.A., 2011, Morphologic clues to the origin of iron-oxide-cemented concretions in the Navajo Sandstone, south-central Utah: The Journal of Geology, v. 119, p. 505–520, doi:10.1086/661110.

Loope, D.B., Kettler, R.M., Weber, K.A., Hinrichs, N.E., and Burgess, D.T., 2012, Rinded iron-oxide concretions: Hallmarks of altered siderite masses of both early and late diagenetic origin: Sedimentology, v. 59, p. 1769–1781, doi:10.1111/j.1365-3091.2012.01325.x.

Lucchitta, I., Holm, R.F., and Lucchitta, B.K., 2011, A Miocene river in northern Arizona and its implications for the Colorado River and the Grand Canyon: GSA Today, v. 21, no. 10, p. 4–10, doi:10.1130/G119A.1.

MacMinn, C.W., and Juanes, R., 2013, Buoyant currents arrested by convective dissolution: Geophysical Research Letters, v. 40, p. 2017–2022, doi:10.1002/grl.50473.

Nielsen, G.B., Chan, M.A., and Petersen, E.U., 2009, Diagenetic coloration facies and alteration history of the Jurassic Navajo Sandstone, Zion National Park, southwestern Utah: Utah Geological Association, v. 38, p. 67–96.

Parry, W.T., 2011, Composition, nucleation, and growth of iron oxide concretions in the Jurassic Navajo Sandstone, Utah: Sedimentary Geology, v. 233, p. 53–68, doi:10.1016/j.sedgeo.2010.10.009.

Parry, W.T., Chan, M.A., and Beitler, B., 2004, Chemical bleaching indicates episodes of fluid flow in deformation bands in sandstones: American Association of Petroleum Geologists Bulletin, v. 88, p. 175–191, doi:10.1306/09090303034.

Parry, W.T., Chan, M.A., and Nash, B.P., 2009, Diagenetic characteristics of the Jurassic Navajo Sandstone in the Covenant oil field, central Utah thrust belt: American Association of Petroleum Geologists Bulletin, v. 93, p. 1039–1061, doi:10.1306/04270908170.

Pederson, J., Karlstrom, K., McIntosh, W.C., and Sharp, W., 2002, Differential incision of Grand Canyon related to Quaternary faulting—Data from U-series and Ar-Ar dating: Geology, v. 30, p. 739–742, doi:10.1130/0091-7613(2002)030<0739:DIOTGC>2.0.CO;2.

Potter, S.L., and Chan, M.A., 2011, Iron mass transfer and fluid flow patterns in Jurassic Navajo Sandstone, southern Utah, U.S.A: Geofluids, v. 11, p. 184–198, doi:10.1111/j.1468-8123.2011.00329.x.

Reiners, P.W., Chan, M.A., and Evenson, N.S., 2014, (U-Th)/He geochronology and chemical compositions of diagenetic cement, concretions, and fracture-filling oxide minerals in Mesozoic sandstones of the Colorado Plateau: Geological Society of America Bulletin, v. 126, no. 9–10, p. 1363–1385, doi:10.1130/B30983.1.

Rowley, P.D., Cunningham, C.G., Anderson, J.J., Steven, T.A., Workman, J.B., and Snee, L.W., 2002, Geology and mineral resources of the Marysvale volcanic field, southwestern Utah: Cedar City, Utah, Geological Society of America Field Guide, Rocky Mountain Section Annual Meeting, p. 131–170.

Shipton, Z.K., Evans, J.P., Dockrill, B., Heah, J., Williams, A., Kirchner, D., and Kolesar, P.T., 2005, Natural leaking CO_2-charged systems as analogs for failed geologic storage reservoirs, *in* Thomas, D.C., and Benson, S.M., eds., Carbon Dioxide Capture for Storage in Deep Geologic Formations, Volume 2, p. 699–712.

Smith, E.L., Sanchez, A., Walker, J.D., and Wang, K., 1999, Geochemistry of mafic magmas in the Hurricane volcanic field, Utah—Implications for small- and large-scale chemical variability of the lithospheric mantle: The Journal of Geology, v. 107, p. 433–448, doi:10.1086/314355.

Utah Geological Survey, 2014, Interactive Geologic Map of Utah, http://geology.utah.gov/maps/geomap/interactive/viewer/index.html.

van der Burg, W.J., 1969, The formation of rattle stones and the climatological factors which limited their distribution in the Dutch Pleistocene, 1. The formation of rattle stones: Palaeogeography, Palaeoclimatology, Palaeoecology, v. 6, p. 105–124, doi:10.1016/0031-0182(69)90007-8.

Watson, M.N., Zwingmann, N., and Lemon, N.M., 2004, The Ladbroke Grove-Katnook carbon dioxide natural laboratory: A recent CO_2 accumulation in a lithic sandstone reservoir: Energy, v. 29, p. 1457–1466, doi:10.1016/j.energy.2004.03.079.

Weber, K.A., Spanbauer, T.A., Wacey, D., Kilburn, M.R., Loope, D.B., and Kettler, R.M., 2012, Biosignatures link microorganisms to iron mineralization in a paleoaquifer: Geology, v. 40, p. 747–750, doi:10.1130/G33062.1.

Wigley, M., Kampman, N., Dubacq, B., and Mickle, M., 2012, Fluid-mineral reactions and trace metal mobilization in an exhumed natural CO_2 reservoir, Green River, Utah: Geology, v. 40, p. 555–558, doi:10.1130/G32946.1.